Contents

Tables

Table

Figures

Figure

Chapter 3

Mechanisms and Observational Signatures of Coronal Dimming

This chapter details the physics of coronal dimming and the observational signatures that result. There are theoretically many physical processes that can lead to an uncareful observer identifying "dimming", which may have little to do with a coronal mass ejection (CME). Traditionally, the term "coronal dimming" has been assumed to refer to the void left in the corona after a CME departs. This is one cause of a transient hole in the corona and is of the greatest concern to space weather forecasters. However, changing temperatures (common during solar eruptive events) cause ionization fraction shifting, resulting in some emissions dimming while others brighten. Additionally, dark material (e.g., a filament) can pass between a bright region (e.g., flaring loops) and the observer, causing a transient dip in emission. Third, solar eruptive events sometimes have associated waves that propagate across the solar disk. These waves are observed as narrow bright fronts with a trailing dark region. The trailing dark region is another way to achieve a transient dimming of emission. Next, there are two ways that Doppler effects can cause transient dips in emission. The first is called Doppler dimming and results from fast moving plasma being sufficiently Doppler-shifted to reduce resonant fluorescence from the solar emission line sources; a phenomenon which is independent of the observation angle. The second occurs if eruptive plasma is moving fast enough in the line-of-sight to shift its emissions outside the bandpass of an observing instrument, which we have named "bandpass dimming". The physics and instrumental identifiers for each of these types of theoretically observable dimming are summarized in Table 3.1 and are discussed in detail in the sections that follow.

Table 3.1: Summary of physical processes that can manifest as observed dimming

Short Name	Physical Process	EVE Observational Identifiers	AIA Observational Identifiers
Mass loss (Fig. 3.1)	Ejection of emitting plasma from corona	Simultaneous intensity decrease in multiple coronal emission lines, with percentage decrease indicative of percentage mass lost	Area over and near the erupting active region (AR) darkens
Thermal (Fig. 3.2)	Heating raises ionization states (e.g., a fraction of Fe IX becomes Fe X); cooling does the opposite	Heating: Emission loss in lines with lower peak formation temperatures and near simultaneous emission gain in lines with higher peak formation temperatures; vice versa for cooling	Heating: Area near AR darkens in channels with lower peak formation temperature and near simultaneous brightening in channels with higher peak formation temperatures; vice versa for cooling
Obscuration (Fig. 3.5)	Dim feature (e.g., filament material) moves into line-of-sight over a bright feature (e.g., flare arcade)	Drop of emission lines proportional to their absorption cross section in the obscuring material	Direct observation of this obscuration process
Wave (Fig. 3.7)	Wave disturbance propagates globally, causing compression/rarefaction of plasma as wave passes by	No effects have been identified	Direct observation of this wave process, especially apparent with difference movies
Doppler (Fig. 3.8)	Fast moving plasma Doppler shifts away from resonant fluorescence with solar emission lines	Doppler wavelength shift of emission lines and change in intensity, possibly also observed as line broadening	Change in intensity of moving plasma as its velocity changes
Bandpass (Fig. 3.9)	Emissions from fast moving plasma have Doppler wavelength shift	Emission line shifts in wavelength or has broadening	Doppler shift convolves with band-pass sensitivity to cause apparent reduction in emission

3.1 Mass-loss Dimming

The physical process in mass-loss dimming is the ejection of emitting plasma (see Figure 3.1; Harrison and Lyons 2000; Harra and Sterling 2001). It can be a CME or a failed ejection, the latter of which still manifests locally as a mass-loss dimming, but does not result in the appearance of a CME in coronagraph data and may not appear in a disk-integrated spectrograph like EVE. The physics model is the standard CME initiation discussed in Section 2.2. However, where most discussions will then follow the CME as it transitions to an interplanetary CME, in mass-loss dimming we are instead interested in the details of the void left behind in the corona. The mass of an average CME and a typical active region are of the same order of magnitude: 10^{15} g, meaning that a departing CME can "blow out" a large part of the active region with it (Aschwanden et al., 2009). This is the physical process assumed to be the main contributor to observed dimming in many recent studies (Sterling and Hudson, 1997; Reinard and Biesecker, 2008, 2009; Aschwanden et al., 2009). Harrison et al. (2003) showed that dimmings can account for a large percentage of CME mass. Thus, mass-loss dimming is very relevant for the space weather community.

Observationally, mass-loss dimming appears in EVE as multiple emission lines dropping nearly simultaneously. In the case of a failed ejection, the dimming area and the ejected mate-

Figure 3.1: Schematic depicting the process of mass-loss dimming. Prior to the eruption (left), coronal loops are relatively quiescent. During and after the eruption (right), the loops are brighter and reconfigured, a CME is ejected, and a void forms in the coronal plasma.

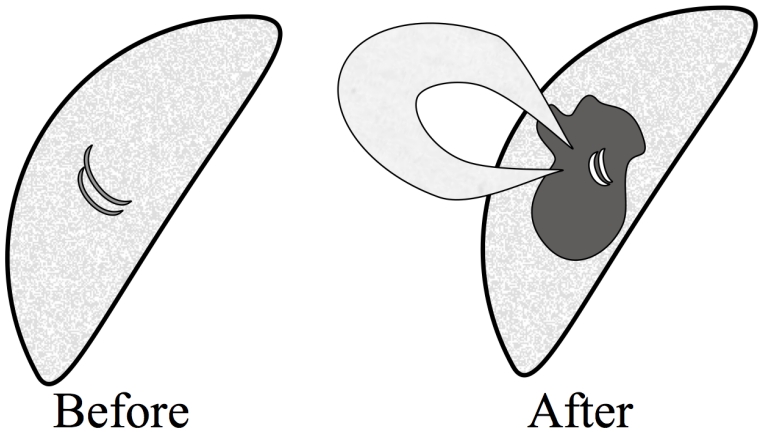

rial are likely to maintain a total emission that is close enough to constant that it will not be apparent in EVE data. For space weather, this is of little concern since CMEs have far greater geoeffectiveness than short-lived holes in the corona of small spatial extent. However, AIA data allow the identification of mass-loss dimming even if the event is a failed ejection. In either case, mass-loss dimming appears in AIA as a relatively compact area near an active region becoming darker, sometimes with a dark cloud visibly moving off-disk. Assuming the dimmings in Reinard and Biesecker (2008) to all be due to mass loss, the timescale of the process is 3 - 12 hr and rarely persists longer than a day. Additional observations from the Hinode spacecraft have confirmed density decreases with accompanying outflows (Attrill et al., 2010; Harra et al., 2010; Tian et al., 2012).

3.2 Thermal Dimming

Figure 3.2: Schematic depicting the observational difference between dimming and non-dimming emission lines. Relative to a pre-eruption time (left), the Fe IX emission drops while the Fe XIV emission increases (right) due to heating of the plasma and redistribution of ionization states.

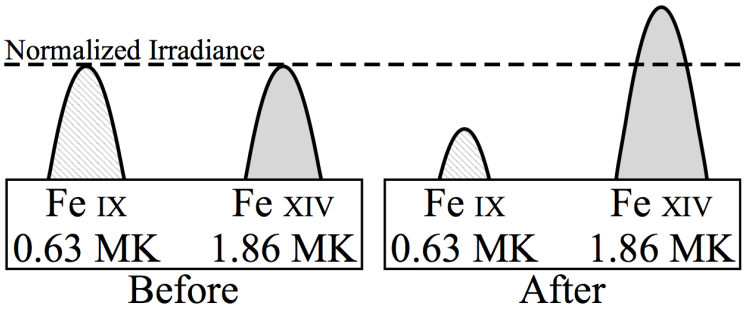

Temperature evolution of emission lines is only interpreted as observed dimming if one is not careful to observe co-spatial emission lines at different peak formation temperatures. As plasma is heated or cooled, the ionization fraction changes, necessarily causing the emission intensity to change (Figure 3.2). For example, heating causes some Fe IX to become Fe X and thus, in the absence of competing physical processes, 171 Å emission drops while 177 Å rises. This pattern was identified observationally in Figure 6 of Woods et al. (2011) using SDO/EVE data, Robbrecht and

Wang (2010) using STEREO/EUVI, and Jin et al. (2009) and Imada et al. (2007) with Hinode/EIS. It can also be observed in the standard composite (multi-wavelength) movies produced by the AIA team; indeed, this is one of the prime purposes for the composites. The initiation time and duration of temperature evolution tends to be quite similar to mass-loss dimming, as they are typically both responses to the rapid release of magnetic field energy in active regions and require several hours of recovery time. Thus, thermal processes could be mistaken for mass loss if only a single spectral line was observed. Ideally, unblended emission lines from an entire coronal ionization sequence (e.g., Fe I to Fe XVIII) could be used to mitigate this convolution of dimming observations. However, as we will show in Section 4.3, it may be sufficient to have observations of two sufficiently separated ionizations states to differentiate between thermal evolution and mass-loss dimming. This is due, in part, to the fact that hotter lines (e.g., Fe XV and above) are primarily emitted from confined loops near the flare and are thus not strongly impacted by mass-loss dimming.

Figure 3.3: Outflow velocity vs emission line peak formation temperature for a dimming region near a plage. Adapted from Imada et al. (2007).

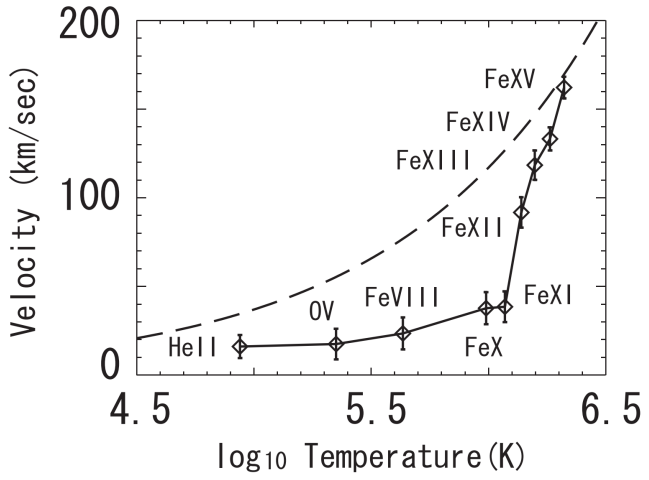

Multi-wavelength Doppler studies have shown that while all (measured) emission lines become blue-shifted (indicating an outflow), the magnitude of the shift is strongly directly proportional to the lines peak formation temperature (Imada et al., 2007; Jin et al., 2009). Figure 3.3 shows this

dependence for a plage region with a dimming during an X-class flare. In particular, Fe IX 171 Å emission can be depressed further after open magnetic field lines from the departing CME close down and cause another bout of heating; causing e.g., Fe IX to become Fe X and beyond, which propagates outward as a "heat wave dimming" (Robbrecht and Wang, 2010). It may even be that cool emissions like Fe IX 171 Å are simply moving too slow to account for mass depletion and that warmer lines, such as Fe XII 195 Å, better represent the mass being ejected (Robbrecht and Wang, 2010). However, Mason et al. (2014) found that the onset time, slope, and duration of dimming are comparable in SDO/AIA 171 Å and 193 Å[1] and in SDO/EVE 171Å and 195 Å (described in Chapter 4).

It is important to note that, in general, the magnitude of total observed dimming in a given line in EVE spectra is inversely proportional to its peak formation temperature, which can be inferred from Figure 3.4. This figure was generated using a simple algorithm that searched all EVE/MEGS-A data for relative irradiance decreases greater than a specified threshold (1%, 2%, 3%) of flares exceeding GOES X-ray class of C1. The window of time searched was bounded by the GOES event start time and the sooner of either 4 hours after the start time or the next GOES event start time. This algorithm was applied to all EVE data from mission start (2010 February 10) to the failure of the MEGS-A instrument (2014 May 26). MEGS-A takes the measurements of all wavelengths studied here. Figure 3.4 shows that the number of dimmings dramatically decreases as the magnitude threshold is increased, and decreases slightly with higher peak formation temperature. This latter effect is partially due to flare heating adding emission in the higher temperature, higher ionization state, lines that partially offsets the mass-loss dimming. Additionally, these trends indicate that at sufficiently high peak formation temperature, no dimming may be observed at all, even at the lowest detection threshold, which is consistent with the hotter lines being restricted to the confined flare loops and hence experiencing no mass loss. In other words, the higher the peak formation temperature, the greater the relative contribution of more confined loops to the measured emission.

[1] Note that the SDO/AIA 193 Å band encompasses 195 Å

Figure 3.4: Number of identified dimmings in EVE for six spectral lines using different percentage dimming depths as the threshold for a detection. There were 263 flares used to trigger an automated search for dimming in EVE. Note the decrease in detections with increasing ionization state (i.e. peak formation temperature).

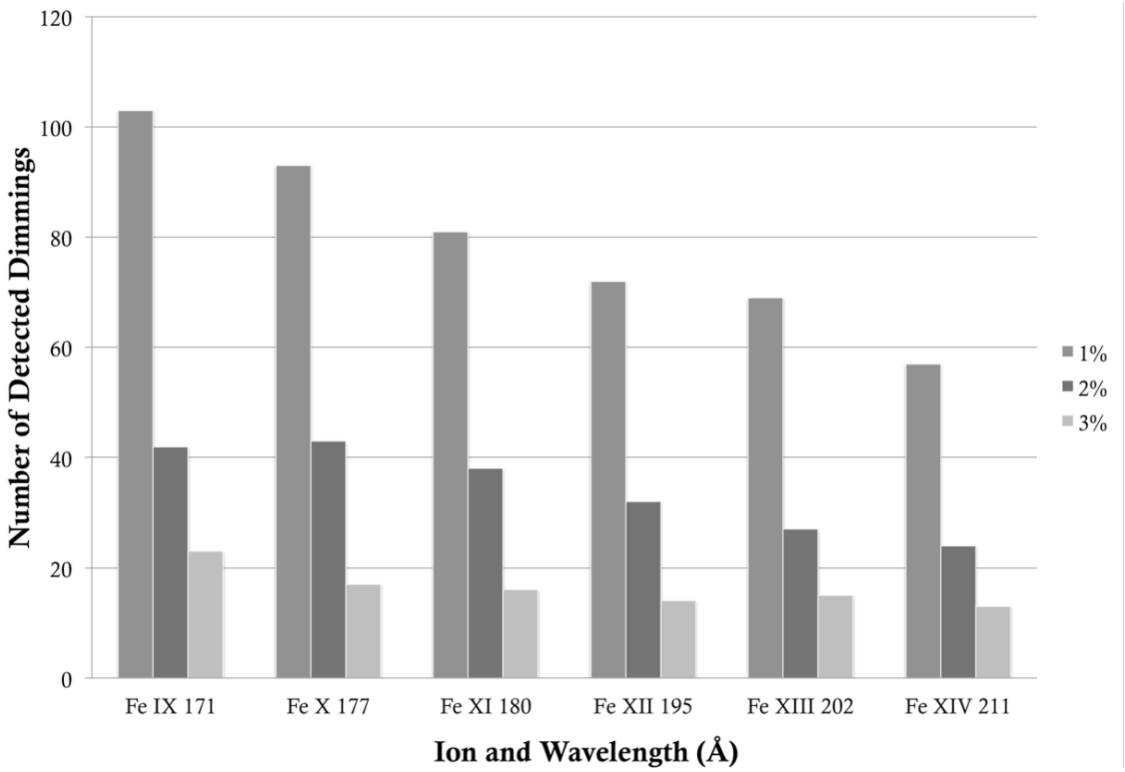

An instrument with spatial resolution like AIA can be used to isolate the confined flaring loops and create a time series of just the dimming region, and this is a procedure carried out in Chapter 4. AIA too has its own limitations; relevant in this case is the relatively lower spectral resolution that blends together emission from several ionization states of Fe. With EVE and AIA combined, it is possible to analyze thermal dimming but the ideal instrument for fully characterizing this phenomenon would be a high-resolution hyperspectral imager in the EUV.

3.3 Obscuration Dimming

The physical process that results in apparent dimming here is material that is dark in a particular wavelength (e.g., a filament) moving between bright material (e.g., flare arcade) and

Figure 3.5: Schematic depicting the process of obscuration dimming. A filament previously obscuring only the quiet Sun (left) expands and moves in front of a flare arcade (right). This results in a decreased observed emission from the flare arcade in wavelengths where the filament is optically thick.

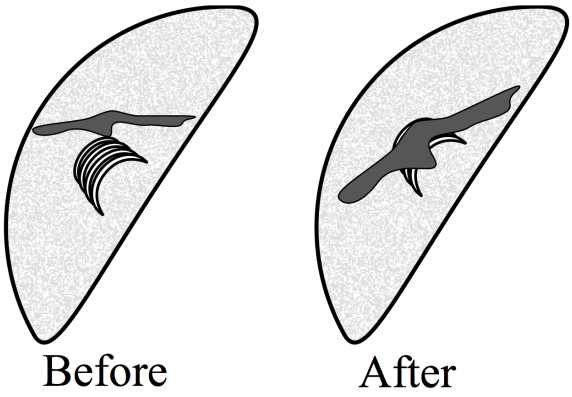

the observer (Figure 3.5). In optically thick wavelengths, the dark plasma absorbs some of the bright emission, resulting in an apparent decrease in emission. The slow draining of plasma back to the corona can obscure underlying emission for hours, and absorption can be observed in both coronal and chromospheric lines (e.g., Gilbert et al. 2013). Although obscuration dimmings can exhibit time and spatial scales comparable to the more short-lived mass-loss dimmings, it is fairly straightforward to identify absorption signatures in the EUV images. It may also be possible to identify this phenomenon with EVE using the He II 256 Å and 304 Å chromospheric emission lines and knowledge of the absorption cross-section through filamentary plasma. Figure 3.6 shows the photoionization cross-sections of the dominant species in the solar corona. Hydrogen and helium contribute an order-of-magnitude more absorption than metals[2] , and thus the effect of metals can be ignored. The cross-sections are quite steep in the wavelength range of interest here (roughly 150-310 Å). This means that approximately twice as much He II 256 Å than He II 304 Å emission will come through a filament. Furthermore, the mass-loss dimming sensitive lines (e.g., Fe IX 171 Å and 195Å) will be less affected by this obscuration, but a 1% effect would be sufficient to cause a "false" detection. It may be possible to identify obscuration dimming with EVE's 256 Å and

[2] "Metals" in the astrophysical sense

304 Å measurements and determine that an obscuration dimming has occurred. However, further analysis of this type of dimming is required before any conclusions can be drawn.

Figure 3.6: Photoionization cross-sections for He I (dot-dashed line), He II (solid line), and H (dashed line) per hydrogen atom. The inset shows a wider wavelength range of the same data but with metals shown for comparison. The dashed vertical bars at the bottom indicate the edges of respective continua. The grey regions at the bottom are not pertinent here as they correspond to specifics of the SOHO/CDS instrument. Adapted from Andretta et al. (2003).

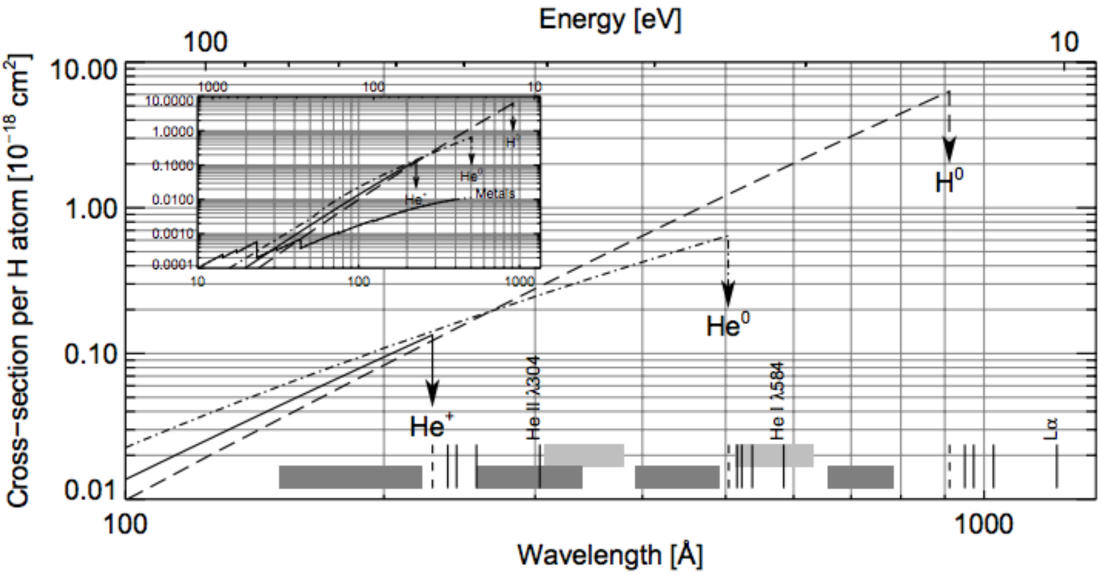

3.4 Wave Dimming

The debate about the physics of coronal EUV waves continues (e.g., Zhukov and Auchère 2004; Muhr et al. 2011; Liu and Ofman 2014) but one of the simplest explanations of the observations is that plasma is compressed as a longitudinal wave passes through the medium. Traveling (i.e., not static) rarefactions are sometimes observed following the compression (Muhr et al., 2011), the compressed regions having higher densities resulting in increased emission, and vice versa (Figure 3.7). Alternatively, some models suggest that the observed phenomenon is not a wave at all, but rather the impact of the CME departing on the global magnetic field (Chen et al., 2002, 2005). Regardless of the physical process responsible, the observation is the same. The EUV waves emanating from an eruption can be seen to cause dimmings and brightenings elsewhere in

the solar EUV images, often very far from the original eruption site, particularly near other active regions. We refer to these dimmings that are non-local to the erupting site as sympathetic dimmings (Schrijver and Higgins, 2015). This is quite likely to occur if a distant active region has significant potential energy stored when the disturbance reaches it – the wave propagating across the magnetic field lines acts as a catalyst.

Figure 3.7: Similar to Figure 3.5, but depicting the process of wave dimming. After an eruptive event, a wave propagates and expands through the corona. The compressed plasma of the wavefront results in enhanced emission, while the rarefied trailing region is dimmed.

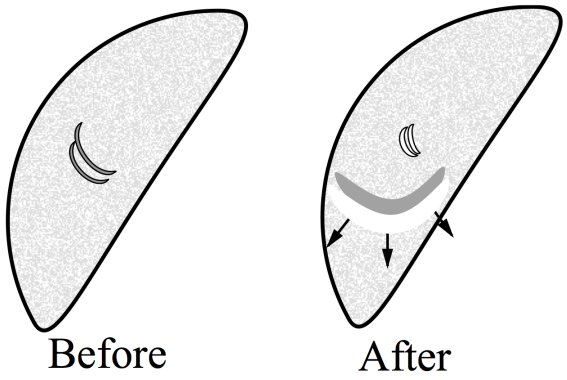

It is important to distinguish between the wave-caused dimmings and other causes of remote dimming, such as large-scale disappearing loops that are visible in soft X-ray images but only have visible EUV changes at their footpoints (Pohjolainen et al., 2005). EUV wave dimmings are unlikely to be easily identified in full-disk spatially-integrated instruments like EVE because the enhanced emission nearly cancels out the dimmed emission when summed.

3.5 Doppler and Bandpass Dimming

Two additional processes can theoretically lead to the observation of dimming in a limited wavelength range and both result from Doppler effects. The first has been given the name "Doppler dimming". In this type of dimming, resonant fluorescence of a high-velocity, remote cloud of plasma (e.g., CME) by a source population (solar emission lines) can decrease as the resultant Doppler shift becomes sufficiently large (see Figure 3.8; Hyder and Lites 1970). Here, Doppler takes effect

due to the relative velocity between the source (the Sun) and the scattering medium (the CME) and is thus independent of observer angle. This phenomenon has been known for decades for cometary emissions (Swings, 1941; Greenstein, 1958) and has been documented in chromospheric lines associated with eruptions (Labrosse and Mcglinchey, 2012) as well as in coronal lines such as O VI for polar coronal hole outflows (Giordano et al., 2000). However, the majority of EUV emission lines in the corona are collisionally dominated i.e. not resonantly excited, and will not exhibit this effect. Furthermore, the dimming region is the CME itself, which is likely to be outside the field of view of EUV instruments observing the solar disk. Therefore, it is possible to diagnose this type of dimming when it is pronounced in resonantly excited lines but does not manifest in the lines of interest studied herein.

Figure 3.8: (a) Geometry of Doppler dimming. The large circle at the bottom represents the Sun, the point P represents the position of mass that has erupted e.g., a CME. The vector V is the velocity of the CME. The square patch on the Sun represents an area of source emission. Adapted from Rompolt (1967). (b) The Hα profiles seen by (A) a stationary observer at a height of 5600 km above the photosphere; and (B) an observer at a height of 30,000 km moving radially outward at 75 $km\ s^{-1}$. The mean intensity (as seen by the scattering medium) is measured in units of the intensity of the nearby continuum at the center of the disk. It can be seen that the Doppler shift also causes an intensity decrease. Adapted from Hyder and Lites (1970).

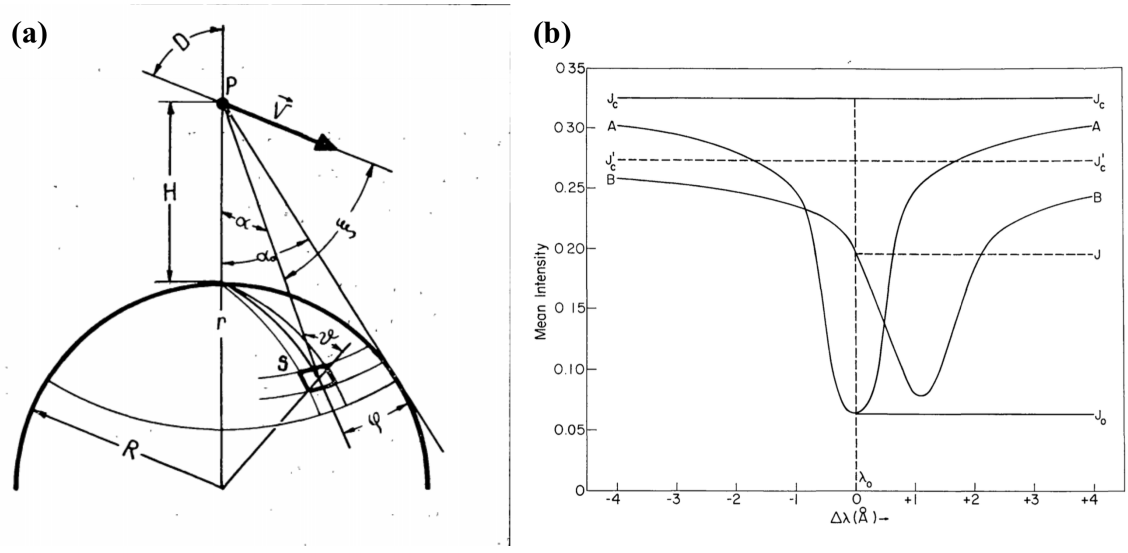

The second type of dimming that results from a Doppler effect is one we call "bandpass

dimming". This physical process is tied to the observers location similarly to obscuration dimming (see Section 3.5). Mass ejected toward the observer will have emissions that are necessarily blue-shifted. If the velocity is high enough, it can shift emission lines outside of an imager's bandpass, causing an apparent dimming in the data. Most imagers use filters that tend to have bandpasses on the order of nanometers but can have sharp edges (Figure 3.9). CMEs typically have speeds ranging from a few hundred to a couple thousand $km\ s^{-1}$. However, a CME only accounts for a small fraction of the total emission from the solar disk. As noted in Hudson et al. (2011), these Doppler shifts tend to be on the order of picometers. Additionally, a CME moving fast enough to shift emission outside the bandpass would be outside the field-of-view of the instrument in a very short time. Thus, this type of apparent dimming is not expected in EUV images, but we include it for completeness and note that this may be a consideration for future instrumentation.

Figure 3.9: (a) and (b) are snapshots from a movie produced by Barbara Thompson. (a) Bottom: The dashed line shows a modeled solar spectrum and the solid line shows the bandpass for AIA's 171 Å. Top left: The ratio of emission relative to plasma with no line-of-sight velocity as a function of velocity. Top right: The amount of density decrease (in %) that would be required to achieve the same amount of dimming as bandpass dimming at each velocity. (b) Same as (a) but at a velocity of 1053 $km\ s^{-1}$.

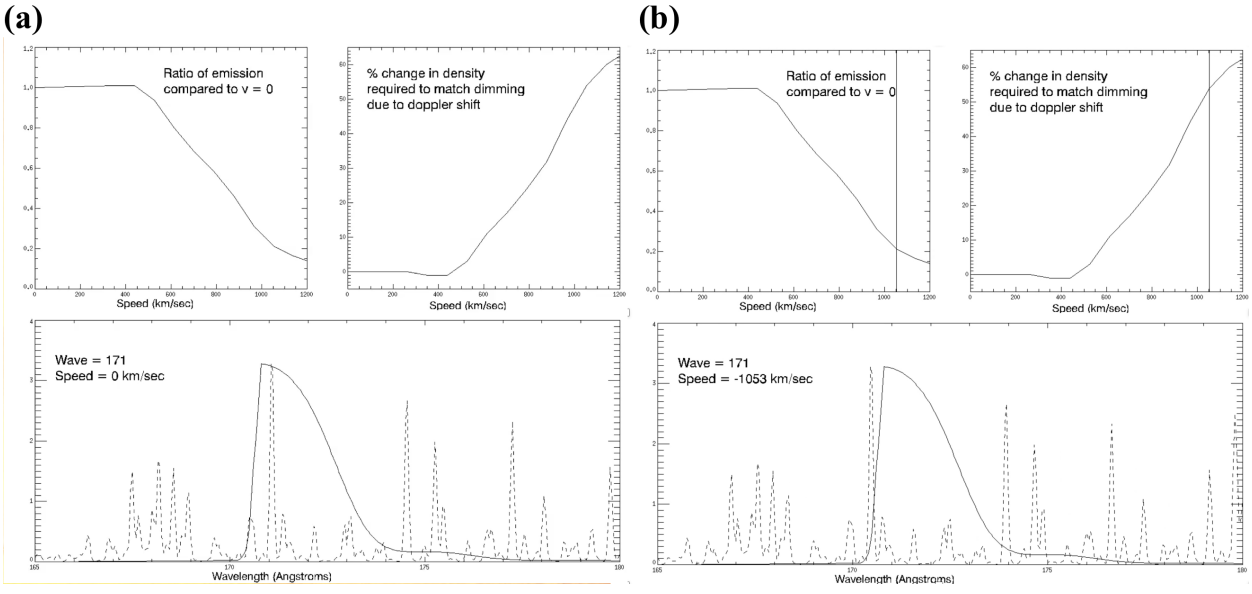

In a spectrograph like EVE, the Doppler shifts would instead simply cause a wavelength

shift of the emission line from the ejected material, which is how Hudson et al. (2011) performed their analysis. When this Doppler-shifted emission is convolved with the relatively static plasma remaining on the Sun, a small Doppler shift from the ejected material manifests as line-broadening in the integrated irradiance while a large shift would result in a line splitting. It should be noted that the EVE extracted lines data product applies a static mask to the spectra so a sufficiently large Doppler shift could cause an apparent dimming in this product. Again, the observed shifts are far too small to impact the EVE data analysis.

3.6 Summary

The physics for most of these types of dimming is relatively simple and well-understood, with the exception of global waves. Mass-loss dimming is simply the direct result of a CME removing a significant quantity of emitting material from the solar corona. This dimming is not immediately lost as the CME pulls away because the post-eruption relaxation period is nonzero and it can take several hours for the quiescent Sun to replace the lost plasma from the surrounding corona and transition region. Instrumentally, even though EUV measurements select specific temperature ranges, mass-estimates based on them appear consistent with white-light coronagraph derived masses (Aschwanden et al., 2009).

Thermal dimming is a major concern in nearly all of the citations above for its potential to interfere with mass-loss dimming and the resultant estimated CME masses. The physics here is also simple: eruptive events result in various forms of heating (see Section 2.2) that shift upward the ionization fraction of dominant EUV emitters (e.g., Fe). Instrumentally, this effect can be compensated for by measuring emission lines from multiple ionization states of the same ion (e.g., Fe IX-XV).

Obscuration dimming physics are also simple, essentially a result of Beer's law, as light passes through a medium with nonzero opacity. Instrumentally, this is easily identified with imagers and we believe it may be possible to identify with a spectrograph, provided some chromospheric helium emission lines are measured (e.g., 256 Å and/or 304 Å).

The physics of global waves is highly contested but the observations are well established. For a disk-integrating spectrograph like EVE, which is the primary source of data analysis herein, we believe that wave dimming will be negated by wave brightening. Indeed, to our knowledge, no observations of waves have been made with EVE.

Doppler dimming physics are well understood and long standing. A CME may fluoresce due to stimulation from the Sun, but the wavelengths will be Doppler shifted according to the relative velocity of the CME from the Sun. This shift reduces the efficacy of the stimulation, resulting in less fluorescence. However, the dimming region in this case is the CME itself, which is likely to be outside the field of view of instruments like AIA and EVE. Additionally, the emission lines of interest in this study are collisionally dominated. Thus Doppler dimming is an interesting phenomenon but is not expected to dramatically impact analyses of the other types of dimming.

The physics of bandpass dimming is simple Doppler shifting of an emitting plasma. Potential dimming in this case is primarily an instrumental effect, as the Doppler shift could push important emission lines outside the instruments bandpass or data processing line-selection masks. However, studies have shown that the actual Doppler shifts are orders of magnitude too small to cause this type of dimming.

Bibliography

Andretta, V., Del Zanna, G., and Jordan, S. D. (2003). The EUV helium spectrum in the quiet Sun: A by-product of coronal emission? Astronomy and Astrophysics, 400(2):737–752.

Aschwanden, M. J., Nitta, N. V., Wuelser, J.-P., Lemen, J. R., Sandman, A., Vourlidas, A., and Colaninno, R. C. (2009). First Measurements of the Mass of Coronal Mass Ejections From the EUV Dimming Observed With Stereo EUVI A + B Spacecraft. The Astrophysical Journal, 706(1):376–392.

Attrill, G. D. R., Harra, L. K., van Driel-Gesztelyi, L., and Wills-Davey, M. J. (2010). Revealing the Fine Structure of Coronal Dimmings andAssociated Flows withHinode/EIS. Solar Physics, 264(1):119–147.

Chen, P. F., Fang, C., and Shibata, K. (2005). A Full View of EIT Waves. The Astrophysical Journal, 622(2):1202–1210.

Chen, P. F., Wu, S. T., Shibata, K., and Fang, C. (2002). Evidence of EIT and Moreton Waves in Numerical Simulations. The Astrophysical Journal, 572(1):L99–L102.

Gilbert, H. R., Inglis, a. R., Mays, M. L., Ofman, L., Thompson, B. J., and Young, C. a. (2013). Energy Release From Impacting Prominence Material Following the 2011 June 7 Eruption. The Astrophysical Journal, 776(1):L12.

Giordano, S., Antonucci, E., and Dodero, M. (2000). OXYGEN VELOCITIES IN A POLAR CORONAL. Advances in Space Research, 25(9):1927–1930.

Greenstein, J. L. (1958). High-Resolution Spectra of Comet MRKOS. The Astrophysical Journal, 128:106.

Harra, L. K., Mandrini, C. H., Dasso, S., Gulisano, A. M., Steed, K., and Imada, S. (2010). Determining the Solar Source of a Magnetic Cloud Using a Velocity Difference Technique. Solar Physics, 268(1):213–230.

Harra, L. K. and Sterling, A. C. (2001). Material Outflows from Coronal Intensity "Dimming Regions" During Coronal Mass Ejection Onset. The Astrophysical Journal Letters, 561:215–218.

Harrison, R. A., Bryans, P., Simnett, G. M., and Lyons, M. (2003). Coronal dimming and the coronal mass ejection onset. Astronomy & Astrophysics, 400:1071–1083.

Harrison, R. A. and Lyons, M. (2000). A spectroscopic study of coronal dimming associated with a coronal mass ejection. Astronomy & Astrophysics, 1108:1097–1108.

Hudson, H. S., Woods, T. N., Chamberlin, P. C., Fletcher, L., Zanna, G. D., Didkovsky, L., Labrosse, N., and Graham, D. (2011). The EVE Doppler Sensitivity and Flare Observations. Solar Physics, 273:69–80.

Hyder, C. L. and Lites, B. W. (1970). H-alpha Doppler Brightening and Lyman-alpha Doppler Dimming in Moving H-alpha Prominences. Solar Physics, 14(1):147–156.

Imada, S., Hara, H., Watanabe, T., Kamio, S., Asai, A., Matsuzaki, K., Harra, L. K., and Mariska, J. T. (2007). Discovery of a Temperature-Dependent Upflow in the Plage Region during a Gradual Phase of the X-Class Flare. Publications of the Astronomical Society of Japan, 59(sp3):S793–S799.

Jin, M., Ding, M. D., Chen, P. F., Fang, C., and Imada, S. (2009). CORONAL MASS EJECTION INDUCED OUTFLOWS OBSERVED WITH HINODE /EIS. The Astrophysical Journal, 702(1):27–38.

Labrosse, N. and Mcglinchey, K. (2012). Plasma diagnostic in eruptive prominences from SDO / AIA observations at 304 Å. Astronomy & Astrophysics, 537:A100.

Liu, W. and Ofman, L. (2014). Advances in Observing Various Coronal EUV Waves in the SDO Era and Their Seismological Applications (Invited Review). Solar Physics, 289(9):3233–3277.

Mason, J. P., Woods, T. N., Caspi, A., Thompson, B. J., and Hock, R. A. (2014). MECHANISMS AND OBSERVATIONS OF CORONAL DIMMING FOR THE 2010 AUGUST 7 EVENT. The Astrophysical Journal, 789(1):61.

Muhr, N., Veronig, A. M., Kienreich, I. W., and Temmer, M. (2011). Analysis of Characteristic Parameters of Large-Scale Coronal Waves Observed by the Solar-Terrestrial Relations Observatory/Extreme Ultraviolet Imager. The Astrophysical Journal, 89:89.

Pohjolainen, S., Vilmer, N., Khan, J. I., and Hillaris, A. E. (2005). Early signatures of large-scale field line opening Multi-wavelength analysis of features connected with a halo CME event. Astronomy & Astrophysics, 434:329–341.

Reinard, A. A. and Biesecker, D. A. (2008). Coronal Mass Ejection-Associated Coronal Dimmings. The Astrophysical Journal, 674:576–585.

Reinard, A. A. and Biesecker, D. A. (2009). The Relationship Between Coronal Dimming and Coronal Mass Ejection Properties. The Astrophysical Journal, 705(1):914–919.

Robbrecht, E. and Wang, Y.-M. (2010). The Temperature-Dependent Nature of Coronal Dimmings. The Astrophysical Journal Letters, 720:88–92.

Rompolt, . (1967). The Hα Radiation Field in the Solar Corona for Moving Prominences. Acta Astronomica, 17.

Schrijver, C. J. and Higgins, P. A. (2015). A Statistical Study of Distant Consequences of Large Solar Energetic Events. Solar Physics, 290(10):2943–2950.

Sterling, A. C. and Hudson, H. S. (1997). YOHKOH SXT OBSERVATIONS OF X-RAY DIMMING ASSOCIATED WITH A HALO CORONAL MASS EJECTION. The Astrophysical Journal, 491:L55–L58.

Swings, P. (1941). Complex Structure of Cometary bands Tentatively Ascribed to the Contour of the Solar Spectrum. Lick Observatory Bulletin, 508.

Tian, H., McIntosh, S. W., Xia, L., He, J., and Wang, X. (2012). What Can We Learn About Solar Coronal Mass Ejections, Coronal Dimmings, and Extreme-Ultraviolet Jets Through Spectroscopic Observations? The Astrophysical Journal, 748(2):106.

Woods, T. N., Hock, R. A., Eparvier, F. G., Jones, A. R., Chamberlin, P. C., Klimchuk, J. A., Didkovsky, L., Judge, D., Mariska, J. T., Warren, H. P., Schrijver, C. J., Webb, D. F., Bailey, S. M., and Tobiska, W. K. (2011). New Solar Extreme-Ultraviolet irradiance Observations During Flares. The Astrophysical Journal, 739:59.

Zhukov, A. N. and Auchère, F. (2004). On the nature of EIT waves, EUV dimmings and their link to CMEs. Astronomy & Astrophysics, 427:705–716.